JOURNAL OF MATERIALS SCIENCE 33 (1998) 241–246

Electro-discharge consolidation of nanocrystalline Nb–Al powders produced by mechanical alloying

C. ROCK, JUN QIU, K. OKAZAKI
Department of Chemical and Materials Engineering, University of Kentucky, Lexington, KY 40506, USA

Nanocrystalline powders of a 77 at% Nb–Al system prepared by mechanical alloying were subjected to external pressures of up to 450 MPa in a ceramic die, producing a green density between 75% and 85% of theoretical. These powders were consolidated into a solid bulk with a relative density of up to 99% by discharging a high-voltage, high-density current pulse (discharge time $< 500\ \mu s$ and input energy of 0.5–1.0 kJ g^{-1}). The consolidated bulk was still a mixture of two nanocrystalline intermetallic phases of Nb_2Al and Nb_3Al. The resultant grain sizes ranged from 13–33 nm. A negative Hall–Petch relation between Vickers microhardness and grain size was clearly observed, indicating that grain-size softening occurs.

1. Introduction

There has been a large amount of work performed recently on producing nanocrystalline powders by mechanical alloying (MA). Very little effort has, however, been made to densify these powders into a useable solid bulk. Karch *et al.* [1] were the first to produce a nanocrystalline TiO_2 solid bulk with densities approaching the theoretical by applying huge external pressures (>1 GPa) to the powders. But these pressures are practically beyond industrial applications. The recent attempt to consolidate nanocrystalline powders was by use of so-called plasma activated sintering (PAS). Tracey and Groza [2] reported for a similar Nb–Al system that PAS at a temperature of 1073–1523 K for 240–840 s yielded grain sizes of larger than 200 nm. This grain size is too large to take advantage of ductilization through the grain-boundary sliding mechanism [3, 4].

Okazaki [5] reported that nanocrystalline Ti–Al and Nb–Al powders could be consolidated into solid bulks by electro-discharge consolidation (EDC) with densities close to theoretical and grain sizes between 12 and 90 nm. The principle of EDC is to discharge a high-voltage (up to 30 kV), high-density current (10 kA cm^{-2}) pulse (for less than 500 μs) from a capacitor bank through the powders under external pressure, resulting in a temperature rise of more than 2500 K, instantaneously to weld nanocrystalline powders together. This discharge time is long enough for densification, yet too short for extensive grain growth as exhibited in the PAS technique. Furthermore, it was found that softening occurred when the grain size decreased below critical values of 22 and 70 nm for Nb–Al and Ti–Al systems, respectively.

In MA of a 77 at % Nb–Al system, a multiphase mixture of niobium, aluminium, Nb_2Al and, Nb_3Al was formed with their grain sizes between 5 and 8 nm [6, 7]. This multiphase mixture could be transformed by annealing at 1373 K for 25.2 ks into a nearly complete Nb_3Al phase with a grain size of approximately 36 nm [8, 9], The present paper concerns with the consolidation of MA powders into a solid bulk without increasing their crystallite sizes by EDC.

2. Experimental procedure

Elemental niobium (77 at %) and aluminium (23 at %) were mechanically alloyed for 1800 ks in a low-energy ball mill at ambient temperature under an argon atmosphere [7]. Powders of a similar composition were also mechanically alloyed in a high-energy planetary mill for 180 ks under an argon atmosphere at ambient temperature [6]. The circuit resistance of the current EDC setup is about 2 mΩ so that, for a reasonable efficiency of a discharge, it is desirable to have a specimen resistance in a range of 10–100 mΩ. Therefore, these MA powders were mixed at a weight ratio of 2.1 in order to produce a suitable resistance of powder specimen under external pressure. The mixed powders were annealed at 823 K for 3.6 ks for strain relief. A 7.3 g powder load was placed into an alumina die with dimensions $0.8\ cm \times 2.5\ cm \times 5.0\ cm$. An MTS hydraulic press was used to apply external pressures of up to 450 MPa. The annealed powders at green densities of 75%, 80%, and 85% of theoretical were discharged with input energies of 0.5, 0.75 and 1.0 kJ g^{-1}, respectively, from a 500 μF capacitor bank. The discharge time was approximately 350 μs. Subsequent X-ray diffraction was taken on a Rigaku diffractometer for 2θ from 20°–80° at a scanning rate of $0.0167^\circ\ s^{-1}$ and a 0.05° scanning interval under 40 kV and 20 mA using a K_α(Cu) wavelength. Density measurements after EDC were performed using the Archimedes principle in distilled water. Vickers microhardness measurements of each consolidated specimen was performed on a Buehler's

0022–2461

microindentation instrument using 300 and 500 g loads with a 12 s holding time. An ISI scanning electron microscope was used at magnifications below $\times 3000$ for microstructural observation of the bulk solids.

3. Results and discussion

Fig. 1 shows the green density and resistance against applied pressure for the mixed powder. This density–pressure curve exhibits a typical powder rearrangement stage during the first 100 MPa, followed by yielding and work-hardening stages. It should be noted that the work-hardening stage is very gradual due to the intrinsic nature of hard nanocrystalline intermetallic powders (5–8 nm). The past EDC experiments [5] indicate that the maximum densification is normally limited to up to nearly 20%. In order to have a reasonably high achieved density ($> 95\%$), the green density should be more than 80%. Secondly, in order to transfer efficiently a discharge energy to the powder for densification, its resistance should be large enough compared to the circuit resistance (2 mΩ). The discharge efficiency is proportional to the specimen resistance divided by the sum of specimen and circuit resistances. In this respect the specimen resistance is preferably more than 18 mΩ (an efficiency greater than 90%). Thirdly, in order to preserve the microstructure inherent in MA powders (nanocrystallinity), there should be a limitation on input energy that can be applied. Accordingly, the experimental conditions are set to have green densities of 75%, 80% and 85% of theoretical, to have specimen resistances of 80, 100 and 130 mΩ and input energies of 0.5, 0.75 and 1.0 kJ g^{-1}, respectively.

The achieved density, ρ_a, after EDC depends upon input energy, E, that is given by $CV^2/2$ where C is the capacitance of a capacitor bank and V the applied voltage to a bank of capacitors, specimen resistance, R_s, that depends on applied pressure, P, green density, ρ_g, that depends also on P, and discharge time, t_d, which depends on C. The achieved density is therefore

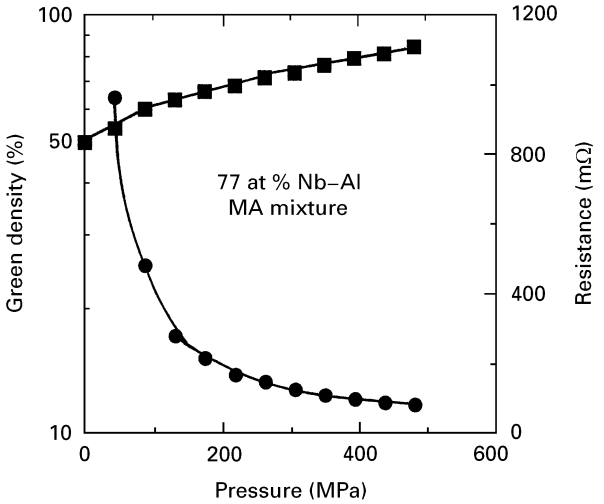

Figure 1 (■) Green density and (●) resistance versus applied pressure for the mixed powders.

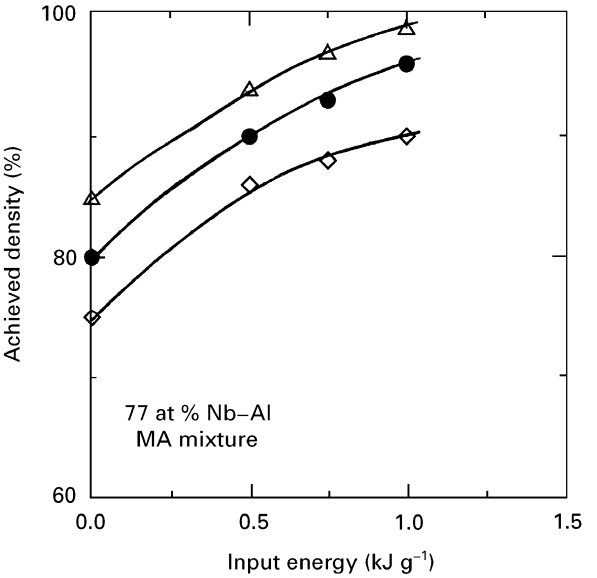

Figure 2 Achieved density versus input energy as a function of green density, ρ_g: (△) 85%, (●) 80%, (◇) 75%.

described by

$$\rho_a = f[\rho_s(P), R_s(P), P, R_c, E(C, V)t_d(C)] \quad (1)$$

where R_c is the circuit resistance. Because R_s and t_d can be fixed, the major variables in Equation 1 are input energy and applied pressure. The densification, $\Delta\rho$ by a discharge is given by

$$\Delta\rho = \rho_a - \rho_g \quad (2)$$

where ρ_g solely depends on pressure. Thus the achieved density and densification mainly depend on input energy once the applied pressure is kept constant.

Fig. 2 shows the achieved density of these powders against the mass-normalized input energy, E/m (kJ g^{-1}) as a function of the specimen resistance (m is the mass of a specimen). As expected, the achieved density increases parabolically with increasing input energy and three curves for three specimen resistances are almost parallel to each other. This implies that densification by EDC is predominantly dependent on input energy, but not on the initial green density. It should be noted that the achieved density could reach up to 99% of theoretical for a 80 mΩ specimen discharged at 1.0 kJ g^{-1}.

To depict clearly this input energy effect on densification, the data in Fig. 2 are converted into a relation between the net densification, $\Delta\rho$, by EDC and input energy normalized for the mass and resistance of a specimen, E_{norm}, which is given by

$$E_{norm} = (E/m)[R_s/(R_s + 2)] \quad (3)$$

where 2 (mΩ) stands for the circuit resistance. In Fig. 3 a single straight line can be drawn through the data points plotted on a log–log scale to yield

$$\Delta\rho_{EDC} = A(E_{norm})^{0.62}\ (\%) \quad (4)$$

where A is an empirical constant dependent on the material used. The exponent 0.62 presently obtained for an Nb–Al nanocrystalline powders is identical to

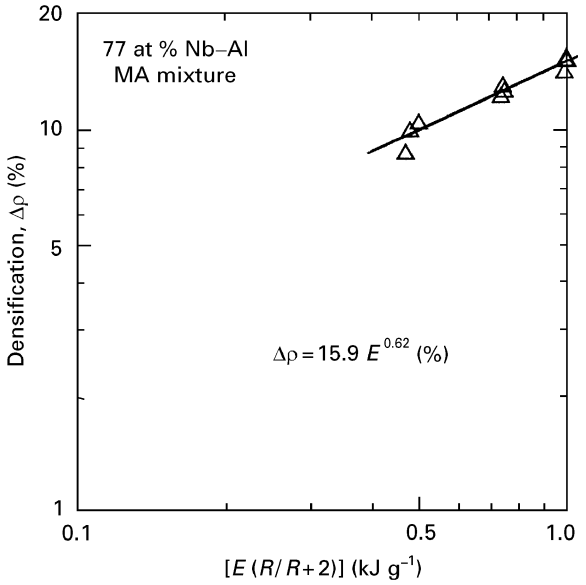

Figure 3 Densification versus input energy normalized for specimen resistance and mass.

that (0.61) previously obtained for Al–8Cr–2Ti powders [10]. This coincidence indicates that the effect of input energy on densification is mainly due to the current EDC setup regardless of materials used. In other words, input energy discharged from a capacitor bank is not transferred 100% to the powder specimen but is partially consumed in the circuit (most probably at the ion switch that produces, upon discharging, plasma between two separated electrodes to close the circuit). The numerical constant A apparently depends on materials; 15.6 for the present material and 9.5 for aluminium based alloy [10]. It is speculated that most probably it may depend on the powder particle size (the smaller the particle size, the greater the numerical constant) that controls the diffusion mechanisms during densification, but the true meaning of this material constant remains to be clarified in the future.

One of the advantages of EDC is the preservation of the original microstructure in MA powders. Because of a very short discharging time, it is expected that no drastic change occurs in the characteristic features of MA powders. The influence of EDC conditions was examined by XRD for EDC compacts. The results are presented in Fig. 4. Here XRD spectra for compacts produced with input energy held constant at 0.5 kJ g^{-1} are shown as a function of specimen resistance along with the as-MA spectrum. Two points of interest should be noted. First, the major peaks are approximately at the same positions as those seen in as-MA powders. All of the spectra appear to be associated with a multiphase mixture due to its complexity [7], indicating that a discharge did not drastically alter the constituting phases. The second point to note is that the largest peak at 38.5° slightly gains intensity with increasing specimen resistance, R_s. This slight change in intensity suggests that a very small amount of grain growth is occurring during EDC at a constant discharge energy of 0.5 kJ g^{-1}. Owing to a minimal change in these spectra, it is concluded that a change

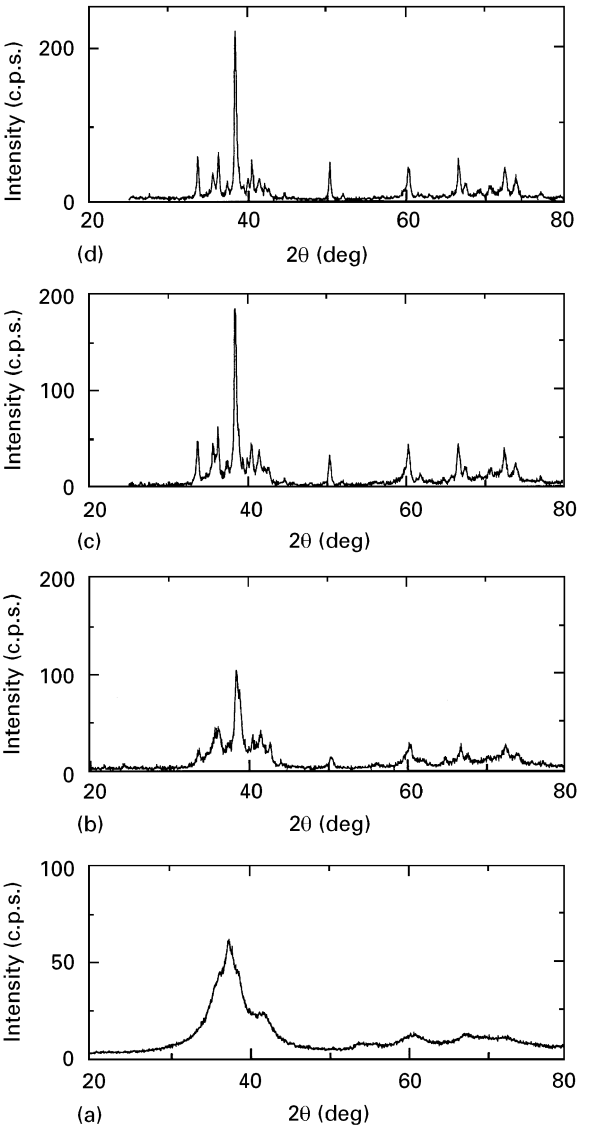

Figure 4 Influence of specimen resistance on XRD spectra of EDC compacts discharged with the same input energy of 0.5 kJ g^{-1}. (a) As–MA 1800 ks, (b) $R = 80$ mΩ, (c) $R = 100$ mΩ, (d) $R = 130$ mΩ.

in R_s (in other words, a change in ρ_g) does not play a major role in altering the characteristic features inherent in the MA state as long as input energy is kept constant at this level.

The effect of input energy on XRD spectra was then examined. Fig. 5 shows the results of XRD after EDC; here the specimen resistance is held constant at 80 mΩ but input energy is increased from 0.5 kJ g^{-1} to 1.0 kJ g^{-1}. Clearly seen here is that an increase in input energy results in a significant increase in the major-peak intensity, although other minor peaks are not influenced very much. Accordingly, it can be concluded that input energy plays a major role in grain growth and there is a possibility of changing the distribution of constituting phases.

Grain growth and phase change during EDC were verified by deconvoluting the XRD spectra obtained for all the EDC compacts. The method of deconvolution involves placing Gaussian curves to represent diffracted peaks within a raw XRD spectrum and performing a non-linear least squares fit to reduce error between the sum of the Gaussian curves and the

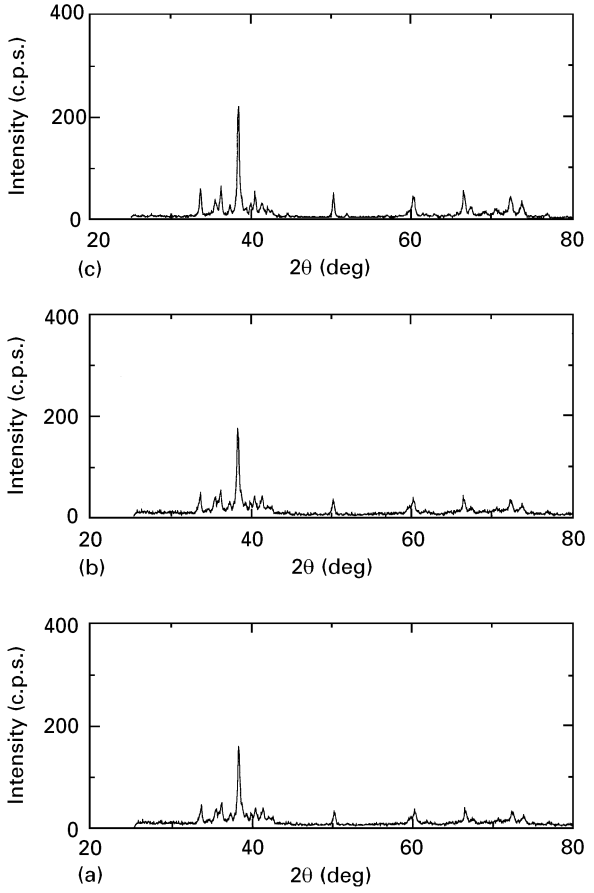

Figure 5 Influence of input energy on XRD spectra of EDC compacts discharged with input energies of (a) 0.5, (b) 0.75 (c) 1.0 kJ g^{-1} by keeping the specimen resistance constant at 80 mΩ.

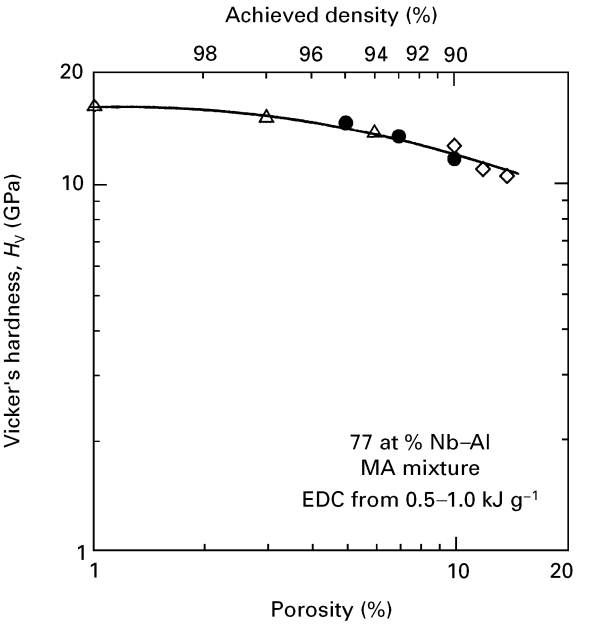

Figure 6 Influence of porosity on hardness of bulk solids produced by EDC. ρ_g: (◇) 75%, (●) 80%, (△) 85%.

raw XRD spectrum [6–9]. The final data obtained after following a strict fitting algorithm are individual peak position 2θ, half-width, B, intensity, I, and area, A, under a peak. Thus a precise phase identification in a multiphase mixture can be made, and the crystallite size and volume fraction of constituent phases are calculated using these data.

The results of deconvolution are presented in Table I. Let us first focus on the crystallite size and volume fraction for the constituent phases. The phases present in MA powders were identified as niobium, aluminium, Nb_2Al and Nb_3Al [7, 8]. In EDC compacts, the existing phases are only Nb_2Al and Nb_3Al except one case (0.5 kJ kg^{-1} for 80 mΩ). The volume fraction of Nb_3Al after EDC increased while that of Nb_2Al decreased, indicating that the transformation of Nb_2Al to Nb_3Al has occurred during a discharge. Also seen is that grain growth has occurred in both these phases. Because the deconvolution results provide the crystallite sizes for these two phases, the average crystallite size, D_{avg}, for an EDC compact is calculated by using a mixture rule

$$D_{avg} = [(D_{Nb_2Al} V_{Nb_2Al} A'_{Nb_2Al}/\rho_{Nb_2Al}) + (D_{Nb_3Al} V_{Nb_3Al} A'_{Nb_3Al}/\rho_{Nb_3Al})] \quad (5)$$

where D, V, A' and ρ are the crystallite size, volume, atomic mass and density of the respective phase, respectively.

The greater the specimen resistance and input energy, the larger the average grain size becomes. Yet the grain growth during EDC is somewhat limited; the grain size increased from 5 nm to the largest size of 32 nm. This limited grain growth is due, in part, to a very short heating time in EDC. These grain sizes after EDC are of the same order found in high-temperature anneal of MA powders [8, 9]. In the same token, the ultimate grain sizes were a direct consequence of complex reactions among the three different phases of different crystal structures existed in as-MA powders.

It is naturally expected that the achieved density will influence mechanical properties of EDC compacts. Hardness of EDC compacts is plotted against the porosity in Fig. 6 on a log–log scale. Surprisingly, the measured hardness is quite high, being between 14.7 and 17.6 GPa. At this moment it is only speculated that high hardness may be due to the presence of two phases in EDC compacts. They may form a complex grain-boundary interface between them, preventing easy grain-boundary sliding. As expected, hardness increases with decreasing porosity almost in a linear manner up to 5% (the relative density of 95%), indicating the contribution of pores to hardness is dominating. Accordingly, higher hardness should be expected by further reducing the pore density. But the data points start to deviate from the linearity when the achieved density exceeds 95%. At this porosity level it is considered that the effect of porosity on hardness should become less significant. Therefore, the reason for deviating from the linearity has to be sought in something else. One possible explanation is the grain-size effect; when the green density is higher, the same input energy produces higher achieved density with smaller grain size (see Table I).

To demonstrate the grain-size effect on hardness, another series of EDC experiments was carried out.

TABLE I The results of deconvolution for grain size and volume fraction of existing phase along with green density, specimen resistance, achieved density, densification and hardness as a function of input energy

E (kJ g^{-1})	ρ_o (%)	R_0 (mΩ)	ρ_{gch} (%)	$\Delta\rho$ (%)	H_v (GPa)	D_{avg} (nm)	D_{Nb_3Al} (nm)	D_{Nb_2Al} (nm)	V_{Nb_3Al} (vol %)	V_{Nb_2Al} (vol %)	V_{Nb} (vol %)
0.5	85	80	94	8.8	13.97	13	14	13	64	31	5
0.75	85	80	97	12.4	14.95	26	28	19	79	21	0
1	85	80	99	14.3	16.67	29	31	22	79	21	0
0.5	80	100	90	10.1	12.35	24	27	20	70	30	0
0.75	80	100	93	13.2	13.23	27	29	23	75	25	0
1	80	100	96	15.4	17.44	32	34	25	84	16	0
0.5	75	130	86	10.6	10.53	26	29	22	69	31	0
0.75	75	130	88	12.8	12.25	31	33	26	74	26	0
1	75	130	90	15.3	13.48	34	37	25	80	20	0

TABLE II Hardness, achieved density and grain-size data for highly densified EDC compacts

H_v (GPa)	ρ (%)	D_{avg} (nm)	$D_{avg}^{-1/2}$ (nm$^{-1/2}$)
13.97	94.2	13	0.277
14.95	97.2	26	0.196
16.17	95.6	27	0.192
16.67	99.1	29	0.185
17.44	96.0	32	0.176
17.84	95.8	34	0.171

Extreme caution was exercised to produce homogeneous packing of MA powders into a die. Thus, higher densities can be achieved even by discharging lower input energies, producing smaller grain sizes. Table II represents these results, where the achieved densities are greater than 95% of theoretical and the average grain sizes are in the range of 12.4–34 nm.

Fig. 7 depicts hardness versus inverse square root of the grain size as according to the Hall–Petch relationship [11]

$$H_v = H_0 + kD^{-1/2} \quad (7)$$

where H_0 is the single crystal strength, k a constant, and D the average grain size of the solid after EDC. It is clearly seen in this figure that a negative Hall–Petch relation exists in EDC compacts when grain sizes are smaller than 34 nm. This signifies softening of the material by grain-size reduction to the nanocrystalline regime allowing some plastic deformation to occur.

Because the EDC compacts are not 100% dense, the hardness may not solely be influenced by grain size. There should exist some relationship between the hardness and two main parameters such as density and grain size. To explore this interdependence, Fig. 8 has been produced where the inverse square root of the grain size, achieved density and hardness are plotted together in three-dimensions. It reveals two very important points. First the negative Hall–Petch relationship undoubtedly exists as seen projected on the hardness–$D^{-1/2}$ plane. Also, there is a separation between the hardness values of samples with high and low densities, indicating the influence of the existing

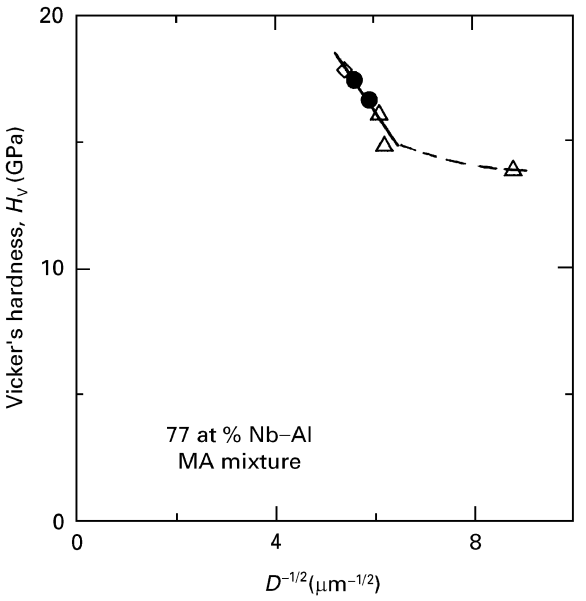

Figure 7 Hardness versus grain size for highly densified EDC compacts. $\rho_{ach} \geqslant 95\%$. ρ_g: (△) 85%, (●) 80%, (◇) 75%.

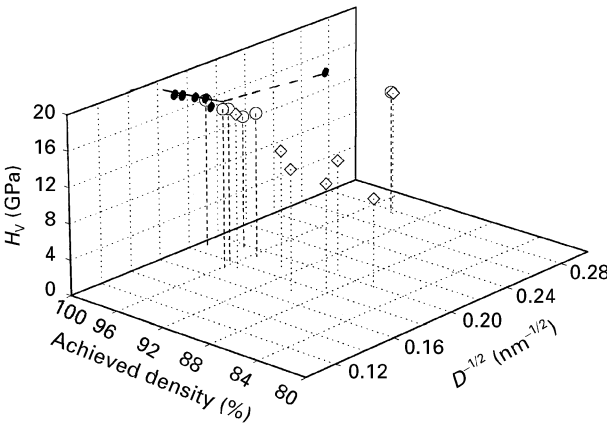

Figure 8 Three-dimensional presentation of hardness, achieved density and inverse square of root of grain size.

pores on this property. When the density is below 95%, the hardness is consistently low, indicating interconnected pores are causing premature fracture. When the density exceeds about 96%, the pores become isolated so that the hardness is exclusively influenced by the solid structure.

To confirm the plastic deformation in these nanocrystalline solids, the hardness indentations were carefully examined by SEM to observe cracks along the indentation edges. It was found that when the hardness increased beyond 16.67 GPa, extensive radial cracks occurred along the indentation boundary, which is typical of brittle failure. But at hardness values below 16.67 GPa, very small radial cracks were infrequently visible at magnifications of $\times 3000$, indicating at least some degree of plastic deformation occurs in these nanocrystalline intermetallic bulk solids.

4. Conclusions

The EDC consolidation of a 77 at% Nb–Al multiphase system resulted in four major findings.

1. EDC has the ability to produce a dual-phase Nb_2–Al–Nb_3Al intermetallic bulk solid with theoretical density of 98% and grain size of 26–36 nm from multiphase powders with a grain size of 5–8 nm.

2. The final phase composition of the bulk solid after EDC is not the same as the initial phase composition of the as-MA powders.

3. The hardness values of the bulk solid are extremely high (14.7–17.6 GPa), indicating very large strength due to the presence of dual intermetallic phases in the bulk solid.

4. The hardness of the solid was decreased by reducing the grain size, exhibiting a negative Hall–Petch relation. Accordingly, some plastic deformation has occurred at hardness values below 16.67 GPa.

References

1. J. KARCH, R. BIRRINGER and H. GLEITER, *Nature* **30** (1987) 556.
2. M. J. TRACEY and J. R. GROZA, *Nanostruct. Mater.* **2** (1993) 411.
3. A. H. CHOLSKI, A. ROSEN, J. KARCH and H. GLEITER, *Scripta Metall.* **23** (1989) 1679.
4. H. CHANG, H. J. HOFLER, C. J. ALSTETTER and R. A. AVERBACK, *ibid.* **25** (1991) 1161.
5. K. OKAZAKI, *Rev. Particulate Mater.* **2** (1994) 215.
6. J. SAIDA, K. OHSAKI, M. UDA and K. OKAZAKI, *Mater. Sci. Forum* **179-81** (1995) 171.
7. C. ROCK and K. OKAZAKI, *Nanostruct. Mater.* **5** (1995) 643.
8. J. SAIDA, Y. TANAKA and K. OKAZAKI, *Trans. JIM.*, **37** (1996) 265.
9. C. ROCK and K. OKAZAKI, *Nanostruct. Mater.* **5** (1995) 657.
10. D. K. KIM and K. OKAZAKI, in "Proceedings of P/M in Aerospace and Defense Technologies", (MPIF, Princeton, NJ, 1991) p. 365.
11. N. J. PETCH, *J. Iron Steel Inst.* **25** (1953) 714.

Received 19 April 1996
and accepted 29 May 1997